PHYSICAL REVIEW B VOLUME 22, NUMBER 10 15 NOVEMBER 1980

Second-order Raman scattering in InAs

R. Carles, N. Saint-Cricq, J. B. Renucci, M. A. Renucci, and A. Zwick
*Lt Laboratoire de Physique des Solides, Associé au Centre National de la Recherche Scientifique, Université Paul Sabatier, 118 Route de nce
Narbonne, 31062 Toulouse Cédex, France*

(Received 15 April 1980)

The second-order Raman spectra of crystalline InAs have been analyzed both at 100 and 330 K to obtain the three irreducible components of the Raman tensor (Γ_1, Γ_{15}, and Γ_{12}). Γ_{12} is found negligible. Γ_1 dominates the 2TA scattering, whereas other regions of the spectra show both Γ_1 and Γ_{15} symmetries. The Γ_1 component is compared with recent calculations of the overtones of the two-phonon density of states based on an overlap-valence-shell model. Good agreement is obtained. Although neutron data are not available, all the bands of the second-order Raman spectra are assigned.

I. INTRODUCTION

Second-order Raman scattering by phonons gives information both on lattice-dynamical and electronic properties. Indeed, one can investigate phonons whose wave vectors span the whole Brillouin zone. Nevertheless, the observed bands yields only sums and differences of frequencies of pairs of phonons for which the sum of the wave vectors is nearly equal to zero. In fact, the experimental data reveal only those which correspond to a high density of states. The high resolution of the Raman technique allows the direct determination of the frequencies with great accuracy, and polarized measurements give information on the symmetry. Moreover, one can also investigate the electronic properties of the material by performing resonant Raman experiments. As in the visible range the coupling of the light with the phonons proceeds through the electronic excitations of the crystal, the detailed study of the resonance allows us to elucidate the nature of the different microscopic processes which govern the scattering mechanism. When the electron-lattice interaction is of the deformation-potential type, values of electron–two-phonon deformation potential are determined.[1,2]

In this paper, we shall be concerned only with the lattice-dynamical aspect. There exist no complete neutron scattering data for InAs due to the large neutron absorption coefficient of In (115 b at $\lambda = 1.08$ Å).[3] As a consequence, the first motivation of this work was to obtain a detailed picture of the phonons in InAs by supplementing the information already gathered by other techniques. Experimental results show that there exists a good correlation between the totally symmetric Γ_1 component of the Raman tensor and the one-phonon density of states in IV and III-V compounds.[4] This work provides, then, an experimental picture of the density of one-phonon states. It enables us also to discriminate between the different theoretical models proposed to describe the lattice dynamics of InAs.[5,6]

The interpretation of the Raman spectra displayed in Sec. II relies on various experimental and theoretical results. The values of the phonon frequencies obtained by techniques other than Raman scattering are discussed in Sec. II. The phonon dispersion curves calculated using different models are shown in Sec. III. In general, structures corresponding to longitudinal phonons do not show up clearly in the second-order Raman spectra. We use a simple linear model to calculate these frequencies at X and L in zinc-blende- and diamond-type materials. The results are presented in Sec. III. The temperature dependence of the intensities of the Raman spectra and the similarities they display with other IV and III-V compounds were very helpful, together with the selection rules deduced from group theory, in assigning unambiguously the structures. These points will be discussed in Sec. IV.

II. EXPERIMENTAL RESULTS

Table I summarizes the experimental determinations of the phonon frequencies in InAs at the high-symmetry points of the Brillouin zone. Also included are the data deduced from the present Raman study.

It should be pointed out that Koteles and Datars,[7] who performed infrared transmission measurements, found that phonons on the hexagonal face of the Brillouin zone contribute to many strong features of the spectra. Very recently, Orlova[8] determined the phonon dispersion curves in InAs along the ⟨100⟩ and ⟨111⟩ directions by diffuse scattering of thermal x rays. The interpretation of the results relies on a model, and the corrections involved introduce uncertainties in the determination of the frequencies. Nevertheless, because of the lack of complete neutron data, these results are very useful. The preliminary measurements performed at 300 K on the Harwell Dido

TABLE I. Experimental determination of phonon frequencies in InAs.

		ir Reflectivity[a]	Raman 1st order[b]	ir Emission[c]	ir Transmission[d]	ir Transmission[e]	Neutrons[f]	X diffusion[g]	Raman 1st and 2nd order (this work)	
	T (K)	4	300	373	300	15	300	300	100	300
Γ	TO	218.9 ± 3	219.6	221	219	225			220.5	217.3
	LO	243.3 ± 2	241.4	246		243			242	238.6
X	TA			111	$TO_1 = 222$	56	52 ± 10	64	54	53
	LA			145	$TO_2 = 214$	178		139	160	160
	TO			212	LO = 196	217		214	218.5	216
	LO			164	LA = 143	207		192	203	
L	TA			73		49.5	47 ± 15	39	44	44
	LA			148		143.5		140	142.5	139.5
	TO			216		218.5		214	218.5	216
	LO			194		205.5		204	203	
K	TA								54	53
	IA								80	78.5
	IIA								153	
W	2					82.5				
	1					77.5			57.5	

[a] M. Haas and B. W. Henvis, J. Chem. Sol. 12, 1099 (1962).

[b] R. C. C. Leite and J. F. S. Scott, Phys. Rev. Lett. 22, 130 (1969).

[c] From Ref. 24.

[d] O. G. Lorimor and W. G. Spitzer, J. Appl. Phys. 36, 1841 (1965).

[e] From Ref. 7.

[f] From Ref. 9.

[g] From Ref. 8.

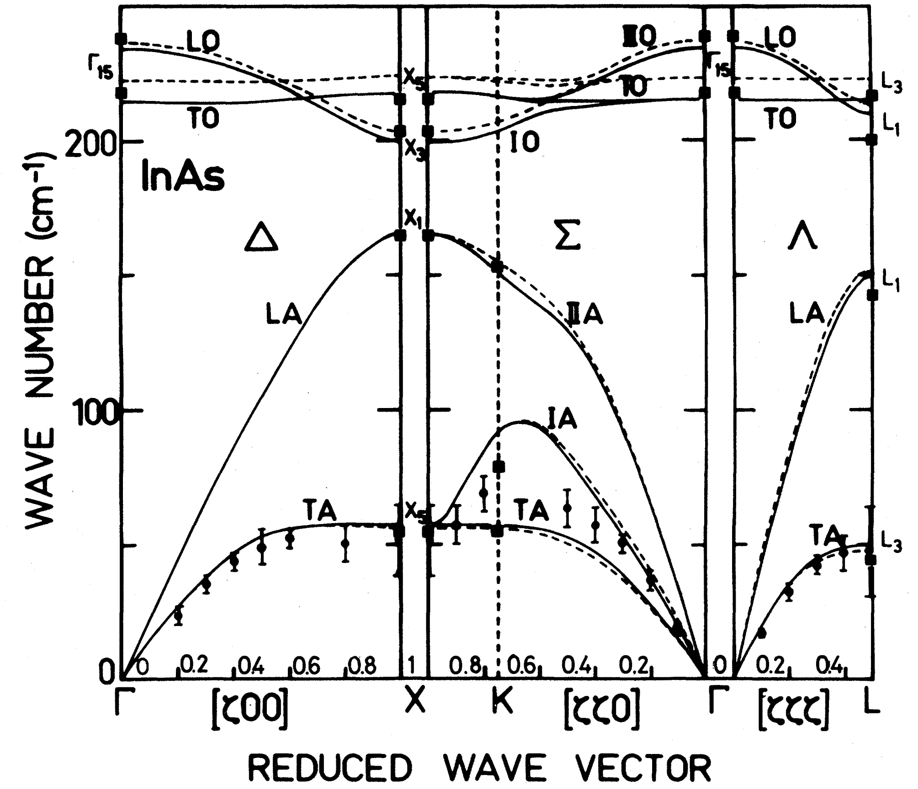

FIG. 1. Calculated phonon dispersion curves of InAs at 300 K from Ref. 6. Dotted lines: model *A*. Full lines: model *B*. Circle: neutron data from Borcherds (Ref. 9) (300 K). Square: Raman data present work (330 K).

3 axis spectrometer by Borcherds[9] are also included in Table I. Only transverse-acoustical branches could be measured and the dispersion curves are presented in Fig. 1.

In our Raman experiments the InAs sample used was an undoped single crystal. The (110) scattering face was x ray oriented to ±2°, mechanically polished and polished etched with Syton. The experiments were performed in the backscattering configuration at room and liquid-nitrogen temperatures; the estimated temperatures are, respectively, 330 and 100 K. Even at room temperature, the spectra were recorded with the sample inside the vacuum chamber of the cryostat to avoid, in the low-frequency region, scattering from air. The two strongest lines of a 164 Spectra Physics argon laser were used, and their power was checked before and after each run. The energy of the 5145-Å line away from the E_1 resonance[10] allows a more significant comparison of the Γ_1 component with the one-phonon density of states. That of the 4880 Å, close to the resonance, enhances the structures of the spectra. We used a T800 Coderg triple spectrometer and the detection was performed with a conventional photon-counting system. The spectra were recorded at low speed (1 cm^{-1} min) and several times to ensure the reproducibility of the measurements. During each run, the Rayleigh line was recorded to determine with precision the energies of the structures and the spectral resolution, which was 3 cm^{-1} for the 5145-Å line and 3.3 cm^{-1} for the 4880-Å line. As usual,[11] in order to extract the three independent components Γ_1, Γ_{15}, and Γ_{12}, we perform four independent measurements, the fourth being used as a check.

Figure 2 displays the results obtained at 330 and 100 K with the 5145-Å line. Figure 3 shows the spectra taken with the 4880 Å at 100 K; the spectra at room temperature have been published elsewhere.[10] The background due to the tail of the Rayleigh scattering has been subtracted in all the spectra. No other correction was performed.

The frequencies quoted in Fig. 3 are reported in Table II together with the ones at 330 K. They are given within 1 cm^{-1} for the strong features, noted *S*, and within 2 or 3 cm^{-1} for the medium and weak ones, noted *m* and *w*. The frequencies of first-order peaks where determined within 0.5 cm^{-1} by recording the Stokes and anti-Stokes components. The symmetries observed experimentally for the different structures are given in Table II

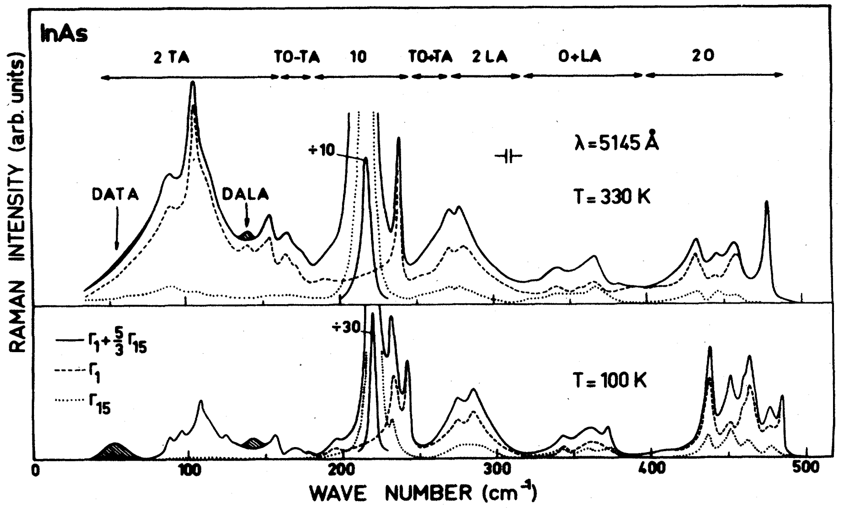

FIG. 2. Second-order Raman spectra of InAs obtained at 100 and 330 K with $\lambda = 5145$ Å. Dashed lines: Γ_1 components. Dotted lines: Γ_{15} components.

together with the ones deduced from group-theoretical arguments by Birman.[12] When the same structure exhibits two types of symmetry the smaller component is given in parenthesis.

III. THEORETICAL DETERMINATIONS OF THE FREQUENCIES

The theoretical values of the frequencies found by Talwar and Agrawal[5] using a rigid-ion model (RIM) and those of Borcherds and Kunc[6] determined with an overlap-valence-shell model (OVSM) are presented in Table III. Model A, proposed by Borcherds and Kunc,[6] was constructed under the assumption that the parameters of the model are obtained by averaging those used for InP and InSb. As replacing one cation by another does not modify significantly the interatomic forces,[13] these authors assumed in model B that the parameters of the model for InAs are equal to those of GaAs. The lattice constant and the atomic masses refer, nevertheless, in model B to InAs. As we shall use the OVS model later in our discussion, we present in Fig. 1 only the phonon dispersion curves deduced from it.

We discuss now the model we used to determine the longitudinal-acoustic and optical frequencies

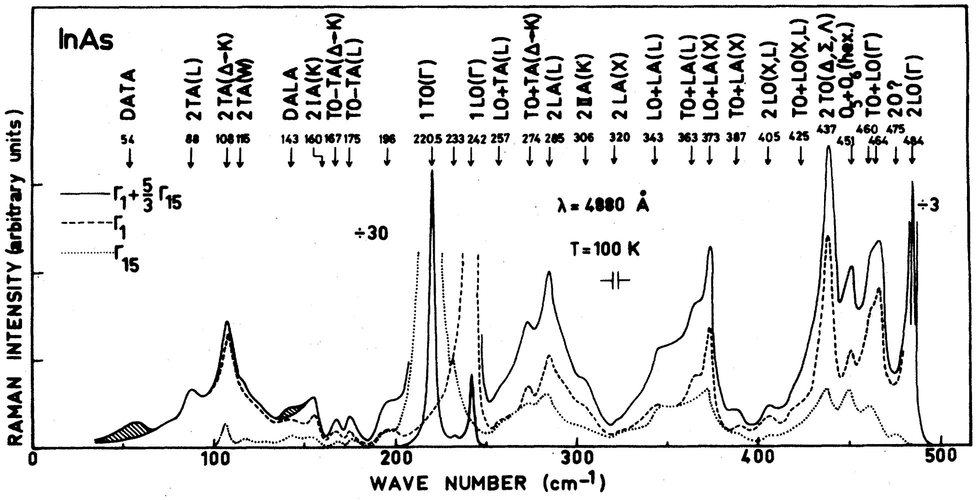

FIG. 3. Second-order Raman spectra of InAs obtained at 100 K with $\lambda = 4\,880$ Å. Dashed line: Γ_1 component. Dotted line: Γ_{15} component.

TABLE II. Characteristic frequencies, in cm^{-1}, of features found in the Raman spectra of InAs and their assignment.

Frequency 100 K	Frequency 330 K	Intensity	Symmetry	Type of singularity	Assignment	Theoretical symmetry[a]
54		*m*			DATA	
88	87.5	*S*	$\Gamma_1(\Gamma_{15})$	P_1	2TA(*L*)	$\Gamma_1+\Gamma_{12}+2\Gamma_{15}$
108	106.5	*S*	Γ_1	P_1P_2	2TA(Δ→ *K*)	$\Gamma_1+2\Gamma_{12}+\Gamma_{15}$
115	112	*w*	Γ_1	P_2	2TA(*W*)	$\Gamma_1+\Gamma_{12}+\Gamma_{15}$
143	143	*m*			DALA	
160	157	*m*	$\Gamma_1(\Gamma_{15})$	P_3	2IA(~*K*)	$\Gamma_1+\Gamma_{12}+\Gamma_{15}$
167	165	*m*	$\Gamma_1(\Gamma_{15})$	P_1P_2	TO-TA(Δ→ *K*)	$\Gamma_1+\Gamma_{12}+\Gamma_{15}$
175	176	*m*	$\Gamma_1\Gamma_{15}$	P_1P_2	TO-TA(*L*)	$\Gamma_1+\Gamma_{12}+2\Gamma_{15}$
196		*m*	Γ_1			
220.5	217.3	*S*	Γ_{15}	P_1P_2	1TO(Γ)	Γ_{15}
233		*w*				
242	238.6	*S*	Γ_1	P_1P_2	1LO(Γ)	Γ_1
257	253	*w*	$\Gamma_1\Gamma_{15}$		LO + TA(*L*)	$\Gamma_1+\Gamma_{12}+2\Gamma_{15}$
274	270	*S*	$\Gamma_1(\Gamma_{15})$	$P_1(P_2)$	TO + TA(Δ→ *K*)	$\Gamma_1+\Gamma_{12}+\Gamma_{15}$
285	279	*S*	$\Gamma_1(\Gamma_{15})$	P_1P_2	2LA(*L*)	$\Gamma_1+\Gamma_{15}$
306		*w*	$\Gamma_1(\Gamma_{15})$		2IIA(~*K*)	$\Gamma_1+\Gamma_{12}+\Gamma_{15}$
320	320			P_3	2LA(*X*)	$\Gamma_1+\Gamma_{12}$
343	339	*m*	$\Gamma_1\Gamma_{15}$	P_1	LO + LA(*L*)	$\Gamma_1+\Gamma_{15}$
363	356	*m*	$\Gamma_1\Gamma_{15}$	P_1	TO + LA(*L*)	$\Gamma_{12}+\Gamma_{15}$
373	365	*S*	$\Gamma_1\Gamma_{15}$	P_1P_2	LO + LA(*X*)	Γ_{15}
387		*w*	$\Gamma_1(\Gamma_{15})$		TO + LA(*X*)	Γ_{15}
405	409	*w*	$\Gamma_1(\Gamma_{15})$		2LO(*L*), 2LO(*X*)	$\Gamma_1+\Gamma_{15};\ \Gamma_1+\Gamma_{12}$
425		*w*	$\Gamma_1\Gamma_{15}$		TO + LO(*L*), TO + LO(*X*)	$\Gamma_{15};\ \Gamma_{12}+\Gamma_{15}$
437	432	*S*	$\Gamma_1(\Gamma_{15})$	P_1P_2	2TO(Δ, Σ, Λ)	$\Gamma_1+2\Gamma_{12};\ \Gamma_1+\Gamma_{12}+2\Gamma_{15}$
451	445	*m*	$\Gamma_1\Gamma_{15}$	P_1P_2	O_5+O_6(hex)	
460	456.5	*S*	$\Gamma_1(\Gamma_{15})$	P_1	TO + LO(Γ)	$\Gamma_1+\Gamma_{12}+\Gamma_{15}$
464		*S*	Γ_1	P_2		
475		*w*	$\Gamma_1\Gamma_{15}$		2O(?)	
484	479	*S*	Γ_1	P_1P_2	2LO(Γ)	Γ_1

[a] From Ref. 16.

TABLE III. Theoretical determination of phonon frequencies in InAs.

			Diatomic linear chain (this work)	RIM[a]	OVSM[b] *A*	OVSM[b] *B*
Γ	TO	Γ_{15}		221	223	215
	LO	Γ_{15}		241	237	234
X	TA	X_5		53	55	57
	LA	X_3	161	145	165	165
	TO	X_5		210	223	216
	LO	X_1	199	199	203	207
L	TA	L_3		34	47	50
	LA	L_1	142	138	151	149
	TO	L_3		214	222	215
	LO	L_1	201	202	213	209
W		W_1		69		
		W_2		71		
		W_3		136		
		W_4		186		
		W_5		211		
		W_6		215		

[a] From Ref. 5. [b] From Ref. 6.

at *X* and *L*. For longitudinal phonons along the Δ and Λ directions, the vibrations of atoms of the same species are identical for planes perpendicular to the phonon wave vectors. The vibrations at *X* and *L* deduced from group theory by Montgomery[14] are pictured in Fig. 4. The planes of the same species moving as a whole, leave us with the problem of the linear diatomic chain. The dynamical matrix is very simple if we take into account only interactions between nearest planes.

Calculations at *X* were performed by Talwar and Agrawal.[15] They used one force constant C_X and express $\omega(\mathrm{LA}(X))$ and $\omega(\mathrm{LO}(X))$ in terms of the elastic constant C_{11}:

$$\omega(\mathrm{LO}(X)) = (8C_{11}a/M_2)^{1/2}, \qquad \omega(\mathrm{LA}(X)) = (8C_{11}a/M_1)^{1/2}, \tag{1}$$

where a is the lattice parameter and M_1 and M_2 the masses of the two kinds of atoms with $M_1 > M_2$. The linear relations between $\omega(\mathrm{LA,LO})$ and $[(C_{11}a)/(M_{1,2})]^{1/2}$ are well satisfied for the IV and III-V compounds as shown in Fig. 5. The experi-

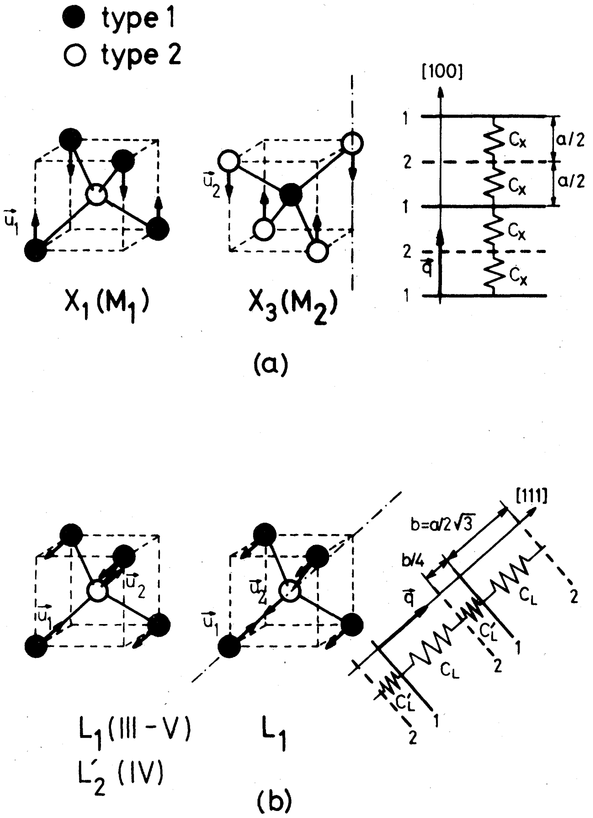

FIG. 4. Symmetry of the longitudinal modes at X (a) and L (b) from Ref. 14. Also sketched are the corresponding diatomic linear models.

mental values used in these plots are listed in Table IV; they correspond to 300 K. The least-squares fit between the experimental points gives a slope (2.64) smaller than the theoretical one ($2\sqrt{2}$). This can be due to the wave-vector dependence of C_X and also to the fact that only interactions between nearest planes were introduced in the model. From Fig. 5, we obtain for InAs at 300 K:

$$\omega(\mathrm{LO}(X))=199\ \mathrm{cm}^{-1},\quad \omega(\mathrm{LA}(X))=161\ \mathrm{cm}^{-1}.$$

In the Λ direction we introduce two force constants C and C' (see Fig. 4). Indeed, although the stretching between plane 1 and its two nearest neighbors, labeled 2, is identical, we must take into account the bending between plane 1 and one set of plane 2 (the bending with the other set is equal to zero). A straightforward resolution of the dynamical matrix at L gives

$$\omega(\mathrm{LO,LA}) =\left\{\frac{C_L+C_L'}{2\mu}\left[1\pm\left(1-\frac{16\mu^2C_LC_L'}{(C_L+C_L')^2M_1M_2}\right)^{1/2}\right]\right\}^{1/2}. \tag{2}$$

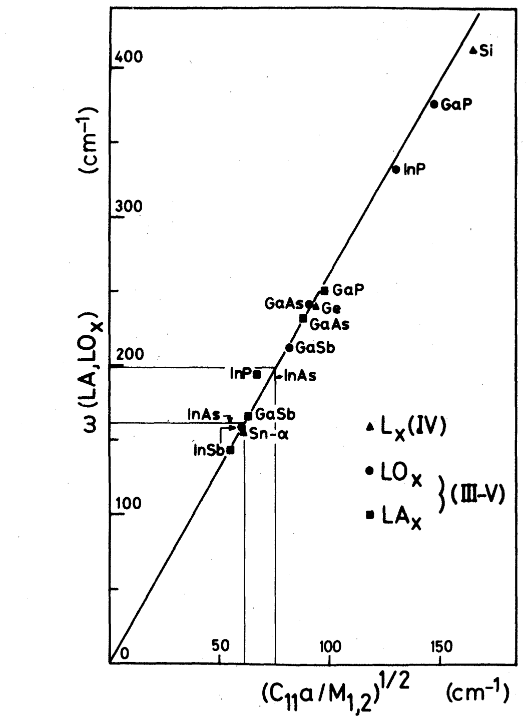

FIG. 5. Frequencies of the longitudinal-acoustic and -optical phonons at X for some diamond- and zinc-blende-type semiconductors as a function of $[C_{11}a)/M_{1,2}]^{1/2}$ expressed in cm^{-1}. The full line is a least-squares fit through the experimental points.

In these expressions, μ denotes the reduced mass. If we suppose that C and C' are wave-vector independent, the resolution of the dynamical matrix for the Γ point gives C_L and C_L' as a function of the elastic constants C_{11}, C_{12}, C_{44} and the lattice parameter a:

$$\begin{pmatrix}C_L\\ C_L'\end{pmatrix}=a\{4C_{11}\pm[4C_{11}(3C_{11}-2C_{12}-4C_{44})]^{1/2}\}. \tag{3}$$

From Eqs. (2) and (3) we get the following relations:

$$[\omega^2(\mathrm{LO}(L))+\omega^2(\mathrm{LA}(L))]^{1/2}=\left(\frac{8C_{11}a}{\mu}\right)^{1/2}, \tag{4}$$

$$[\omega(\mathrm{LO}(L))\omega(\mathrm{LA}(L))]^{1/2} =\left(\frac{16C_{11}(C_{11}+2C_{12}+4C_{44})a^2}{M_1M_2}\right)^{1/4}.$$

The plots of Figs. 6 and 7 show that the linearity displayed by Eq. (4) is well satisfied for IV and III-V compounds. Here too the theoretical slopes ($2\sqrt{2}$ and 2) are larger than the experimental ones. The same arguments as the ones invoked for the X point can explain this discrepancy. From Figs. 6 and 7, we deduce for InAs at 300 K

TABLE IV. Experimental data used for the plots of Figs. 5, 6, 7, and 9. a(Å) is the lattice parameter. C_{11}, C_{12}, and C_{14} in units of 10^{10} Pa are the elastic constants. M_1 and M_2 are the atomic masses and μ the reduced mass, and ω in cm^{-1} are the phonon frequencies.

Material	Sn − α	Ge	Si	GaSb	GaAs	GaP	InSb	InAs	InP
a[a]	3.245	2.828	2.715	3.059	2.8268	2.7253	3.2395	3.018	2.9343
C_{11}[a]	6.90	13.15	16.57	8.849	11.877	14.11	6.669	8.329	10.22
C_{12}[a]	2.93	4.94	6.39	4.037	5.372	6.187	3.645	4.526	5.76
C_{44}[a]	3.62	6.84	7.96	4.325	5.944	7.043	3.02	3.959	4.60
M_1	118.69	72.59	28.09	121.75	74.92	69.72	121.75	114.82	114.82
M_2				69.72	69.72	30.97	114.82	74.92	30.97
μ	59.35	36.30	14.04	44.33	36.11	21.44	59.09	45.34	24.39
$\omega(\mathrm{TO}(\Gamma))$[a]	200.1 ± 2	298	522	227.1 ± 1	268.6 ± 0.3	366.8	179.8		304.2
$\omega(\mathrm{LO}(\Gamma))$[a]				237.1 ± 1	291.9 ± 0.3	402.8	190.8		346.2
$\omega(\mathrm{LA}(X))$	155.8 ± 2[b]	230 ± 13[c]	411 ± 7[d]	166.4 ± 3.3[e]	226.8 ± 2[f]	250 ± 4[g]	143 ± 3[b]		193.5 ± 10[h]
$\omega(\mathrm{LO}(X))$				211.8 ± 4.3[e]	240.8 ± 15[f]	366 ± 12[g]	158 ± 7[b]		332 ± 3[h]
$\omega(\mathrm{LA}(L))$	138.4 ± 1.3[b]	215 ± 10[c]	378 ± 10[d]	153.4 ± 3[e]	208.8 ± 3[f]	212 ± 8[g]	127.1 ± 2[b]		167 ± 3[h]
$\omega(\mathrm{LO}(L))$	163.1 ± 2.7[b]	247 ± 10[c]	420 ± 11[d]	205.1 ± 4[e]	238.5 ± 2.3[f]	374 ± 8[g]	161 ± 3[b]		340 ± 10[h]

[a] K. Kunc, Ann. Phys. 8, 319 (1973).

[b] D. L. Price, J. M. Rowe, and R. M. Nichlow, Phys. Rev. B 3, 1268 (1971).

[c] G. Nilson and G. Nelin, Phys. Rev. B 3, 364 (1971).

[d] G. Nelin and G. Nilson, Phys. Rev. B 5, 3151 (1972).

[e] M. K. Farr, J. C. Traylor, and S. K. Sinha, Phys. Rev. B 11, 1587 (1975).

[f] J. L. Waugh and G. Dolling, Phys. Rev. 132, 2410 (1963).

[g] L. L. Yarnell, J. L. Warren, R. G. Wenzel, and P. J. Dean, *Neutron Inelastic Scattering* (IAEA, Vienna, 1968), Vol. 1, p. 301.

[h] P. H. Borcherds, G. F. Alfrey, D. H. Saunderson, and A. D. B. Woods, J. Phys. C 8, 2022 (1975).

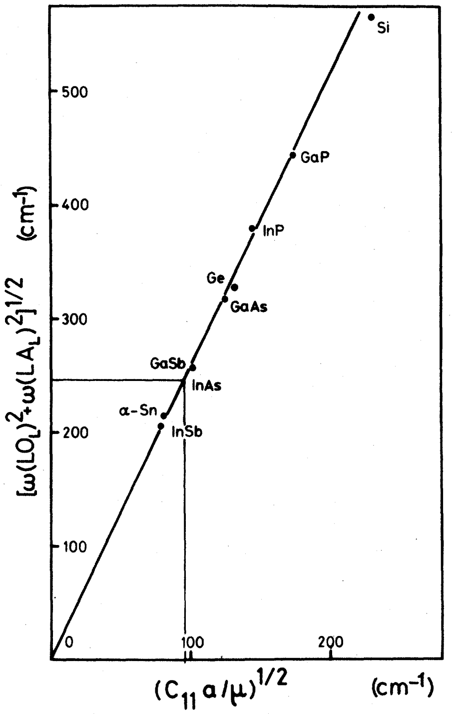

FIG. 6. Plot of $(\omega_{LO}^2+\omega_{LA}^2)^{1/2}$ at L for some diamond- and zinc-blende-type semiconductors as a function of $[(C_{11}a)/\mu]^{1/2}$ expressed in cm⁻¹. The full line is a least-squares fit through the experimental points.

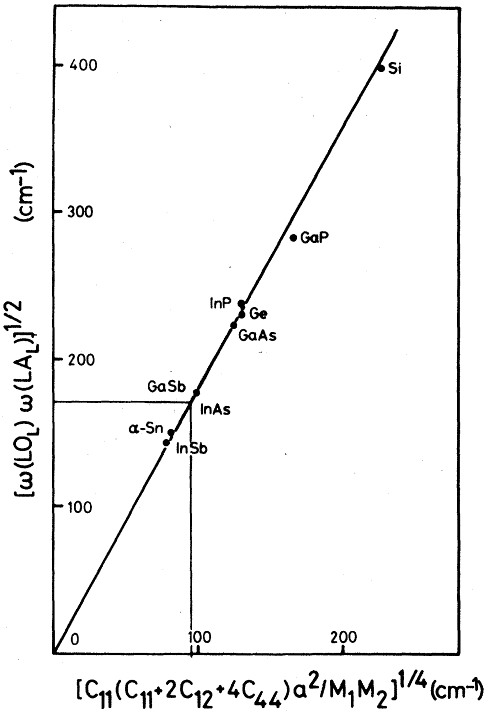

FIG. 7. Plot of $(\omega_{LO}+\omega_{LA})^{1/2}$ at L for some diamond- and zinc-blende-type semiconductors as a function of $[C_{11}\ (C_{11}+2C_{12}+4C_{44})a^2/M_1\,M_2]^{1/4}$ expressed in cm⁻¹. The full line is a least-squares fit through the experimental points.

$$\omega(\mathrm{LO}(L))=201\ \mathrm{cm}^{-1},\quad \omega(\mathrm{LA}(L))=142\ \mathrm{cm}^{-1}.$$

The agreement between the values of the frequencies for the longitudinal phonons at X and L calculated with the linear model and those deduced from full lattice-dynamics calculations is satisfactory (see Table III). Nevertheless, one should note that the values found with the simple linear model are in better agreement with the Raman determination. The simple linear model gives good results since it respects the symmetry of the vibrations at X and L. Also the hypothesis of interactions between nearest planes is not drastic as dynamical properties are mainly governed by short-range interactions.

IV. ASSIGNMENTS OF THE RAMAN SPECTRA

The trends already observed for others III-V compounds[16] appear in Figs. 2 and 3:

(i) Within the experimental uncertainties the Γ_{12} component is negligible compared to the Γ_{15} and Γ_1 components.

(ii) The Γ_1 component dominates all the spectral range [except around the TO(Γ) which is of Γ_{15} symmetry].

(iii) The Γ_{15} component is very weak in the low-frequency region, which corresponds to overtones of transverse-acoustic phonons, but contributes significantly to combination processes (250–280 cm⁻¹ and 320–380 cm⁻¹).

We shall discuss successively the different features of the spectra. We refer to Fig. 3 where the spectra are enhanced by resonance effects.[10]

10 band. The two strong features at 220.5 and 242 cm⁻¹ correspond to first-order TO(Γ) and LO(Γ) peaks. The experimental geometry implies an allowed TO(Γ) and a forbidden LO(Γ) if one uses the conventional selection rules for wave-vector–independent scattering. Nevertheless, the LO(Γ) is allowed in the Γ_1 component if the selection rules are derived for "forbidden scattering." The two kinds of selection rules were checked within 5%. This supports the hypothesis of true backscattering in the sample. It implies also a correct orientation of the crystal and a negligible depolarization ratio of the light.

20 band. The scattering between 400 and 490 cm⁻¹ is due to second-order optical processes. The peak at 484 cm⁻¹ corresponds to the 2LO(Γ). Although the density of states should be equal to zero, this structure appears under resonance conditions (see Figs. 2 and 3). The peak at 437 cm⁻¹

has a frequency somewhat smaller than that of twice the TO(Γ). As its symmetry is mainly Γ_1 it is attributed to overtones of transverse modes. We label it 2TO(Δ, Σ, Λ). This confirms the flatness of the transverse-optical branches in these directions given by the theoretical models of Borcherds and Kunc.[6] The strong feature below the 2LO(Γ), located at 456.5 cm^{-1} at 330 K, is resolved in two components at 100 K and corresponds to the TO + LO(Γ). The structure at 451 cm^{-1}, which contains also a large Γ_{15} component, is consistent with the assignment of Koteles and Datars.[7] The feature at 405 cm^{-1} mostly of Γ_1 symmetry is a good candidate for the 2LO(*L*) or the 2LO(*X*) as suggested by theoretical estimations (Table III). These assignments conform with the crossing of the longitudinal- and transverse-optical branches deduced from arguments related to ionicity.[17] The weak shoulder at 425 cm^{-1}, which contains an appreciable amount of Γ_{15} component, can be attributed to the TO + LO(*L*) and TO + LO(*X*).

2TA band. The low-frequency region between 80 and 160 cm^{-1} mostly of Γ_1 symmetry is attributed to overtones of transverse-acoustic phonons. The shape of the spectrum and the singularities observed correspond fairly well with the ones found for the IV compounds[11,18] and other III-V compounds. Figure 8 displays the similitude between the transverse-acoustic branches of InSb, InP, and InAs. They are compared with the overtones of two-phonon density of states of Ref. 8. For InSb and InP second-order Raman spectra have already been investigated by other authors.[19,20] Figure 8 suggests the simple scaling law $\omega(\text{InAs}) = \frac{1}{2}[\omega(\text{InSb}) + \omega(\text{InP})]$. The results found in this way for the TA(*X*), TA(*L*), and the IA(*K*) in InAs are in good agreement with our Raman data as shown in Table V. The structures at 88 and 157 cm^{-1} are attributed to the 2TA(*L*) and 2IA(~*K*), respectively. The strong peak at 108 cm^{-1} is labeled 2TA(Δ → *K*) as it is due to the excitation of TA-phonon overtones in a region extending from half of the Δ direction to the *K* point of the Brillouin zone. Its large intensity reflects essentially the flatness of the transverse-acoustic branches in these directions. The OVS model[6] predicts well this flatness whereas the RI model[5] is less satisfactory. Recent neutron measurements on GaP[21] have shown that the transverse-acoustic branches around the *W* point are flat and higher in energy than the transverse-acoustic one along Δ and Σ. Consequently, the shoulder at 115 cm^{-1} is attributed to the 2TA(*W*).

DAA (disorder-activated acoustic). Two broad features are observed in the low-frequency region at 54 ± 4 cm^{-1} and 143 ± 4 cm^{-1}. They are shaded in Figs. 2 and 3. As shown by Carles *et al.*,[22] they correspond to disorder-induced first-order scattering. The structure at 54 cm^{-1} was labeled DATA (disorder-activated transverse-acoustic). It coincides with the maximum of the density of states of transverse-acoustic phonons, which implies phonons around *X*. In the same manner, the feature at 143 cm^{-1} mirrors the density of states of the longitudinal-acoustic phonons and was labeled DALA (disorder-activated longitudinal-acoustic). In this case the maximum of the density of states corresponds to phonons around *L*. One should notice that the assignment of the

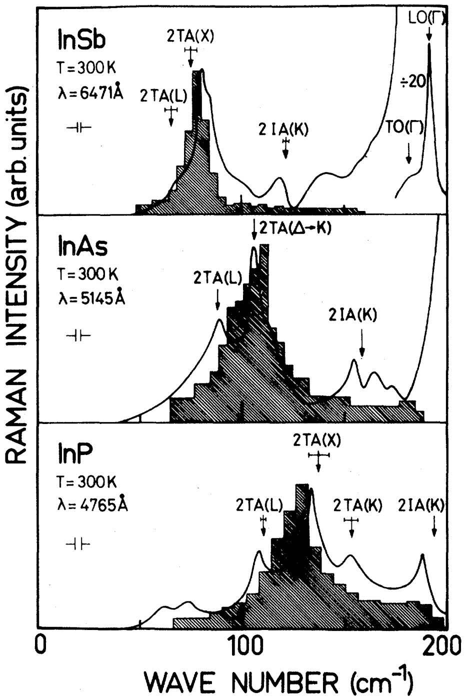

FIG. 8. Second-order acoustic Raman spectra of InSb, InAs, and InP compared with the overtones of two-phonon density of states calculated with the OVS model of Ref. 6.

TABLE V. Characteristic phonon frequencies, in cm^{-1}, of the acoustic-phonon spectra of InSb, InP, and InAs.

	InSb $T = 300$ K[a]	InP $T = 300$ K[b]	$\frac{\text{InSb} + \text{InP}}{2}$	InAs $T = 330$ K[d]
TA(*L*)	32.7 ± 1.7	55 ± 0.6	43.9 ± 1.2	43.8 ± 0.5
TA(*X*)	37.4 ± 1.7	68.4 ± 3	52.9 ± 2.4	53.2 ± 0.5
IA(~*K*)	60.7 ± 0.7	97 ± 1[c]	78.9 ± 0.8	78.5 ± 0.5

[a] D. L. Price, J. M. Rowe, and R. M. Nichlow, Phys. Rev. B 3, 1268 (1971).

[b] P. H. Borcherds, G. F. Alfrey, D. H. Saunderson, and A. D. B. Woods, J. Phys. C 8, 2022 (1975).

[c] From Ref. 30.

[d] This work.

DATA band is compatible with that of the $2\mathrm{TA}(\Delta \rightarrow K)$ already discussed.

TO-TA branch. The structures at 167 and 175 cm^{-1} are attributed to difference combinations for the following reasons: Their intensities decrease rapidly with temperature,[22] the contribution of Γ_{15} is important, and such structures appear in the difference in the density of states calculated by Borcherds and Kunc.[6] These structures are assigned to the $\mathrm{TO\text{-}TA}(\Delta \rightarrow K)$ and $\mathrm{TO\text{-}TA}(L)$, respectively, in relatively good agreement with our previous assignments.

O + TA and O + LA bands. The shoulder at 257 cm^{-1} and the peak at 274 cm^{-1} are attributed to additive combinations. We interpret the last structure as the $\mathrm{TO} + \mathrm{TA}(\Delta \rightarrow K)$. All the features between 340 and 390 cm^{-1} contain an appreciable component of Γ_{15} symmetry and are attributed to additive combinations of optical and longitudinal-acoustic phonons.

2LA band. The maximum of the band around 285 cm^{-1} coincides with twice the calculated frequency of the $\mathrm{LA}(L)$; it has a large-Γ_1 component and we assign it to the $2\mathrm{LA}(L)$. The shoulder at 306 cm^{-1} corresponds to the $2IIA(\sim K)$ as suggested by the OVS model.[6] The frequency of the $\mathrm{LA}(X)$ predicted by the linear chain model or the OVS model[6] brings the $2\mathrm{LA}(X)$ in the deep around 325 cm^{-1}. The singularity of type P_3 found experimentally favors this assignment in accordance with the one deduced theoretically.[23]

The assignments of the second-order Raman spectra presented above are in good concordance with those deduced from other experimental techniques. The only discrepancy concerns the values of the frequencies of the $\mathrm{TA}(X)$ and the $\mathrm{TA}(L)$ given by Stierwalt and Potter.[24] Because a strong absorption band hides the structures below 160 cm^{-1} in the experiments of Koteles and Datars,[7] we believe that our values of the frequencies for the $\mathrm{TA}(X)$ and $\mathrm{TA}(L)$ are more accurate.

The structures at 196, 233, and 257 cm^{-1}, which lie in the strong *10* band, could not be well resolved. The features at 196 and 257 cm^{-1} could be due to As-As band as their frequencies are equal to those of the E_g and A_{1g} modes of crystalline arsenic.[25] The one at 257 cm^{-1} corresponds nevertheless to the $\mathrm{LO} + \mathrm{TA}(L)$ but this assignment should be regarded as tentative. The peak at 233 cm^{-1} is too narrow to be attributed to second-order scattering or to a LO-plasmon mode.[26] We could not assign the feature at 475 cm^{-1}, visible in the *20* band when the spectra are recorded with the 5145-Å line (Fig. 2).

The frequencies proposed for InAs at Γ, L, and X agree with the Brout-sum rule. Mitra and Marshall[27] have shown that, for diamond and zinc-blende structures, this sum is given by

$$S = \sum_{i=1}^{6} \omega_i^2(q) = 24a/\mu\chi\,, \tag{5}$$

where a is the lattice parameter, μ is the reduced mass, and χ is the compressibility; $\chi = [3/(C_{11} + 2C_{12})]$. Relation (5) has been checked for some zinc-blende materials. As shown in Fig. 9 it is well satisfied for the L point. A systematic trend is noted: $S(X) > S(L) > S(\Gamma)$. We point out that the same ordering was found by Rosenstock[28] in diamond and was attributed to "trace-variable" forces.

The frequencies of the phonons located at Γ, X, L, and around K found in this Raman work are plotted in Fig. 1. Among the two models proposed by Borcherds and Kunc[6] the one labeled B (GaAs-like) gives the best agreement. We compare in Fig. 10 the one-phonon density of states, calculated at 300 K by Borcherds and Kunc[6] using model B, with the $\Gamma_1 + 4\Gamma_{12}$ spectrum recorded at 330 K using the 5145-Å line to avoid resonance effects. As mentioned before Γ_{12} is negligible; the experimental spectrum reflects then the Γ_1 component. The histogram reproduces the quantity $C(\omega)g(\omega/2)[\bar{n}(\omega/2) + 1]^2$, where g is the calculated one-photon density of states, $\bar{n}$ is the

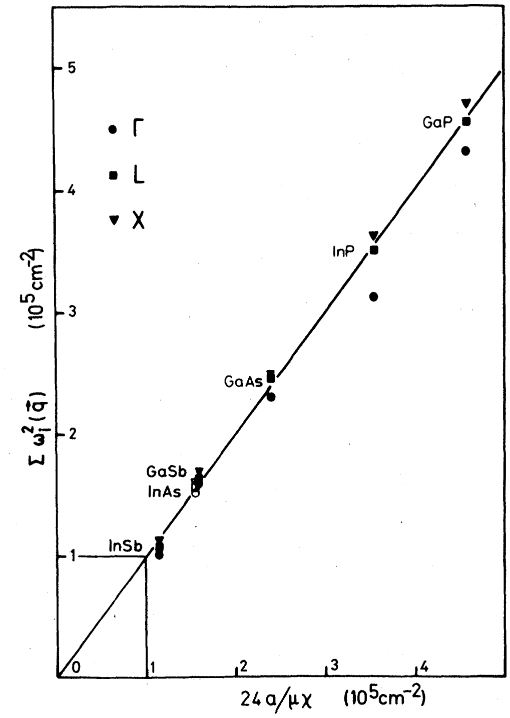

FIG. 9. Brout-sum rule in units of $10^5\ \mathrm{cm}^{-2}$ at Γ, X, and L for some zinc-blende-type semiconductors as a function of $24a/\mu\chi$ given also in units of $10^5\ \mathrm{cm}^{-2}$. The full line is the theoretical plot [Eq. (5)].

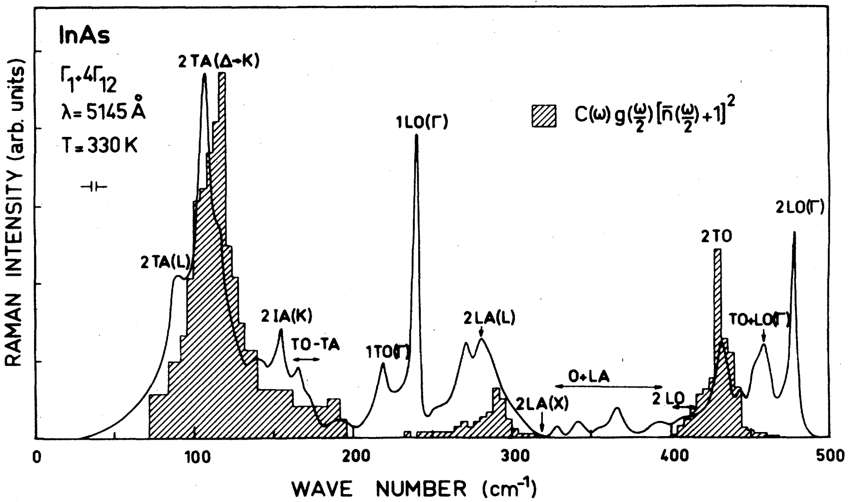

FIG. 10. $\Gamma_1+4\Gamma_{12}$ second-order spectrum of InAs observed at 330 K with $\lambda=5145$ Å compared with the overtone of two-phonon density of states calculated in Ref. 6 and weighted by the $C(\omega)\,[\bar{n}\,(\frac{1}{2}\omega)+1]^2\,g(\frac{1}{2}\omega)$ (see text).

Bose-Einstein factor, and $C(\omega)$ is a correction factor to account for the optical properties[29] of the sample and the spectral response of the setup

$$C(\omega)=\frac{1-R(\omega_s)}{\alpha(\omega_i)+\alpha(\omega_s)}\,\frac{\omega_s^4}{n(\omega_s)}f(\omega_s,\vec{e}_s)\,.$$

R, α, and n are the reflection coefficient, the absorption coefficient, and the index of refraction, ω_i and ω_s refer to the incident and scattered light with $\omega_s=\omega_i+\omega$, $\vec{e}_s$ is the polarization vector, and $f(\omega_s,\vec{e}_s)$ is the response function of the system.

For clarity, we did not include in the histogram the combined two-phonon sum and two-phonon difference in the density of states. As a consequence the structures around 170 and 330–380 cm^{-1}, which where attributed to combinations, are not reproduced although they appear in the calculations of Ref. 6. Of course, the 1LO(Γ) and the TO + LO(Γ) peaks which correspond to forbidden processes cannot be accounted for. Apart from these points, there is a general correspondence between Γ_1 and the overtones of the density of states showing that all the modes of Γ_1 symmetry contribute equally to the corresponding Raman tensor. A better agreement could be achieved, in particular in the acoustic region, by shifting to lower energies the calculated density of states. The main discrepancy concerns the density of states for the longitudinal-acoustic branch near L. Such a large experimental contribution was also found in the Raman spectra of the $\mathrm{InAs}_x\mathrm{P}_{1-x}$ alloys system.[30]

---

[1] B. A. Weinstein and M. Cardona, Phys. Rev. B 8, 2795 (1973).

[2] M. A. Renucci, J. B. Renucci, R. Zeher, and M. Cardona, Phys. Rev. B 10, 4309 (1974).

[3] J. E. Bacon, *Neutron Diffraction* (Clarendon, Oxford, 1962).

[4] See, for example, P. B. Klein and R. K. Chang, Phys. Rev. B 14, 2498 (1976).

[5] D. N. Talwar and Bal. K. Agrawal, Phys. Status Solidi B 63, 441 (1974).

[6] P. H. Borcherds and K. Kunc, J. Phys. C 11, 4145 (1978).

[7] E. S. Koteles and W. R. Datars, Can. J. Phys. 54, 1676 (1976).

[8] N. S. Orlova, Phys. Status Solidi B 93, 503 (1979).

[9] P. H. Borcherds (private communication).

[10] R. Carles, N. Saint-Cricq, M. A. Renucci, and J. B. Renucci, in *Lattice Dynamics*, edited by M. Balkanski (Flammarion, Paris, 1978), p. 195.

[11] B. A. Weinstein and M. Cardona, Phys. Rev. B 7, 2545 (1973).

[12] J. L. Birman, in *Handbuch der Physik*, edited by L. Genzel (Springer, Berlin, 1974), Vol. XXVb.

[13] N. Meskini and K. Kunc (private communication).

[14] H. Montgomery, Proc. R. Soc. London A309, 521 (1969).

[15] D. N. Talwar and Bal K. Agrawal, Phys. Rev. B 8, 693 (1973).

[16] M. Cardona, in *Light Scattering in Solids*, Topics in Applied Physics, edited by M. Cardona (Springer, Berlin, 1976), Vol. 8, p. 1.

[17] R. W. Keyes, J. Chem. Phys. 37, 72 (1962).

[18] P. A. Temple and C. E. Hathaway, Phys. Rev. B 7, 3685 (1973).

[19] W. Kiefer, W. Richter, and M. Cardona, Phys. Rev. B 12, 2346 (1975).

[20] G. F. Alfrey and P. H. Borcherds, J. Phys. C 5, L275 (1975).

[21] P. H. Borcherds, K. Kunc, G. F. Alfrey, and R. L. Hall, J. Phys. C 12, 4699 (1979).

[22] R. Carles, N. Saint-Cricq, and J. B. Renucci (unpublished).

[23] F. A. Johnson and R. Loudon, Proc. R. Soc. London A281, 274 (1964).

[24] D. L. Stierwalt and R. F. Potter, Phys. Rev. 137A, 1007 (1965).

[25] W. Richter, T. F. Fjeldly, J. B. Renucci, and M. Cardona, in *Lattice Dynamics*, edited by M. Balkanski (Flammarion, Paris, 1978), p. 104.

[26] S. Buchner and E. Burstein, Phys. Rev. Lett. 33, 908 (1974).

[27] S. S. Mitra and R. Marshall, J. Chem. Phys. 41, 3158 (1964).

[28] H. B. Rosenstock, Phys. Rev. 129, 1961 (1963).

[29] H. R. Philipp and E. Ehrenreich, Phys. Rev. 129, 1550 (1963).

[30] R. Carles, N. Saint-Cricq, J. B. Renucci, and R. J. Nicholas, J. Phys. C 13, 899 (1980).